HHS Public Access

Author manuscript

J Phys Chem Lett. Author manuscript; available in PMC 2016 December 17.

Published in final edited form as:

J Phys Chem Lett. 2015 December 17; 6(24): 4986–4990. doi:10.1021/acs.jpclett.5b02323.

"Size-Independent" Single-Electron Tunneling

Jianli Zhao[†], **Shasha Sun**[‡], **Logan Swartz**[§], **Shawn Riechers**[†], **Peiguang Hu**[‖], **Shaowei Chen**[‖], **Jie Zheng**[*,‡], and **Gang-yu Liu**[*,†,§]

[†]Department of Chemistry, University of California, Davis, California 95616, United States

[‡]Department of Chemistry, The University of Texas at Dallas, Richardson, Texas 75080, United States

[§]Biophysics Graduate Group, University of California, Davis, California 95616, United States

[‖]Department of Chemistry and Biochemistry, University of California, Santa Cruz, California 95064, United States

Abstract

Incorporating single-electron tunneling (SET) of metallic nanoparticles (NPs) into modern electronic devices offers great promise to enable new properties; however, it is technically very challenging due to the necessity to integrate ultrasmall (<10 nm) particles into the devices. The nanosize requirements are intrinsic for NPs to exhibit quantum or SET behaviors, for example, 10 nm or smaller, at room temperature. This work represents the first observation of SET that defies the well-known size restriction. Using polycrystalline Au NPs synthesized via our newly developed solid-state glycine matrices method, a Coulomb Blockade was observed for particles as large as tens of nanometers, and the blockade voltage exhibited little dependence on the size of the NPs. These observations are counterintuitive at first glance. Further investigations reveal that each observed SET arises from the ultrasmall single crystalline grain(s) within the polycrystal NP, which is (are) sufficiently isolated from the nearest neighbor grains. This work demonstrates the concept and feasibility to overcome orthodox spatial confinement requirements to achieve quantum effects.

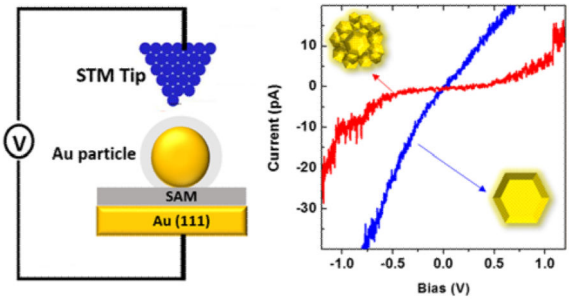

[*]**Corresponding Authors** G.-L.: Tel: (530) 754-9678. Fax: (530) 754-8557. gyliu@ucdavis.edu. J. Z.: Tel: (972) 883 5768. jiezheng@utdallas.edu. .

Notes

The authors declare no competing financial interest.

Single-electron tunneling (SET), correlated one-by-one transfer of electrons through a Coulomb Island such as a metallic nanoparticle, offers a unique property for future single-electron devices.[1–8] Coulomb Blockade (CB) and Coulomb Staircase (CS) are the two most well-known characteristics of SET.[9,10] Scanning tunneling microscopy (STM) and spectroscopy (STS) have proven to be accurate test platforms for SET and conductance/capacitance measurements,[3,10–15] where the two electrodes and tunneling junction are shown in Figure 1B. SET is only found for nanoparticles satisfying two necessary conditions: (a) $E_C > k_BT$ (the charging energy, $E_C = e^2/2C$, associated with the addition of one electron to an island with capacitance C must exceed the thermal energy, k_BT, to surpass thermally activated electron tunneling) and (b) $R > 6.5$ kΩ (the tunneling resistances (R) of the junctions must be larger than the quantum resistance, $h/4e^2$ (~6.5 kΩ) to reach the required signal-to-noise ratio with respect to quantum fluctuations of electrons).[6,16] At room temperature $k_BT = 26$ meV, and thus C must be on the order of 10^{-18} F or smaller to fulfill $E_C > k_BT$. Considering metallic nanoparticles, the capacitance is correlated with particle size, $C = 2\pi d\varepsilon_0\varepsilon$, where ε is the dielectric constant of the coating, d represents the particle's diameter, and ε_0 is the vacuum permittivity constant.[6,17] Therefore, it must be that $d < 10$ nm to exhibit SET at room temperature; in fact, most SET have been seen for particles of only a few nanometers.[2,6,7,16,18–22] To observe SET for particles above 10 nm, cryogenic temperatures were required, which has made device applications less practical.[8,10,16] Moreover, in SET reported previously, the CB and CS voltages depend on the size of the NPs.[8,10]

In this work, we demonstrate the breaking of the aforementioned size requirements. The evidence comes from the observation of SET at room temperature using Au NPs with metallic core size as large as 20 nm. The breakthrough is rationalized by the unique intraparticulate structure: the presence of single crystalline grains ($\ll$10 nm), isolated by dielectric surroundings. The results open the paradigm that it is feasible and likely to attain SET at room temperature using NPs whose size serves the convenience of the device's design and fabrication instead of being limited by the intrinsic size-requirements for SET. Therefore, the findings bring SET-based device development a giant step forward. In addition, this work implies that quantum effects can be observed among objects whose size pertains to classic mechanics.

A current versus voltage *(I–V)* spectrum for a polycrystalline Au NP is shown in Figure 1A, where CB and CS are clearly visible at room temperature. The width of the CB ranges from −0.50 to 0.56 V. The corresponding dI/dV shown in gray confirms the presence of a CB and reveals a rich local density of states at the junction, for example, a CS near −0.75 V, and multiple features and peaks between −0.7 and 1.2 V. This nanoparticle has an overall diameter of 21.2 nm. To verify that these observations were genuine and accurate, technical precautions were rigorously taken. First, all STM imaging and *I–V* acquisitions were carried out under ultrahigh vacuum (UHV) to prevent contamination and ensure accuracy, following protocols established by us[6] and by other researchers.[9,23] The key components, including the two electrodes and an NP immobilized via a self-assembled monolayer (SAM), are illustrated schematically in Figure 1B. Second, prior to each *I–V* measurement, STM images were taken to guide the tip to park above the center of the selected NP. Then, a current-

distance (*I*–*Z*) curve was acquired to designate the separation (e.g., 0.03 nm for the *I*–*V* in Figure 1A) between the tip and the top of the NP. Accurate location of the STM tip with respect to the NP is essential for the accuracy and reproducibility of the *I*–*V* measurements.[6,24] Third, the *I*–*V* of the surrounding SAM was acquired, serving as an internal reference. As shown in Figure 1A, the *I*–*V* of the SAM is consistent with prior investigations and does not exhibit a CB or CS.[6,25,26] The *I*–*V* characteristics of internal references confirmed that the STM tip was clean and that the *I*–*V* measurements were carried out accurately.

The appearance of SET for this large NP is very counterintuitive at first glance because 21.2 nm far exceeds the maximum size (10 nm) known to exhibit SET at room temperature.[2,7,16,18] Among tens of Au NPs measured in four sets of independent experiments, 50% of the population exhibited SET behaviors. Intrinsically different from previous Au NPs with SET behavior, our particles are a new class of nanomaterials known as polycrystalline Au NPs, which consist of many smaller single-crystalline nanostructures within.[27,28] The solid-state glycine matrices method yielded NPs with a narrow size distribution, revealed from our careful atomic force microscopy (AFM) imaging, STM measurements, as well as transmission electron microscopy (TEM) characterization. The overall diameter of these immobilized NPs including their coating measures 20.9 ± 0.9 nm, while the metal core is slightly smaller 20.0 ± 0.9 nm. We refer to this type of nanomaterial as P20 NPs hereafter. The fact that 50% instead of 100% P20 NPs exhibit SET behaviors is consistent with the differences in intraparticulate structure among the P20 NPs, also addressed in a later section. In the case of SAM regions, the forward and reverse *I*–*V* curves are almost superpositioned with a small difference of 4.3 pA at zero bias. In the case of P20 NPs, the forward and reverse *I*–*V* curves were almost overlapped, with a small difference of 4.4 pA at zero bias. This near reversibility suggests that no permanent damage occurred to the particle during the measurements.[10]

Positive and negative control experiments were carried out and compared with the P20 NPs to demonstrate the robustness of our observations. The result from a typical positive control experiment is shown in Figure 2, where an Au NP with an 1.5 nm core reveals a CB from −0.45 to 0.45 V, consistent with our previous finding.[6] The 1.5 nm Au core is single-crystalline according to TEM fringes, and thus these NPs are referred to as S1.5 NPs. To facilitate surface adhesion they were modified by mixed dithiol and alkanethiol SAMs, resulting in 2.5 nm in overall diameter.[29] Among tens of these ultrasmall NPs measured, all (100%) revealed SET behavior. In contrast, the negative control was performed using Au NPs with almost identical core size as the P20 NPs, with the *I*–*V* measurements revealing no SET characteristics (see Figure 2). The core size of the individual NPs studied as a negative control as calculated from the calibrated STM height is 20.0 nm, almost equal to that of P20. These conventional NPs are referred to as C20 NPs. Among all tens of C20 NPs tested, none (0%) revealed SET behavior. In contrast, P20 NPs exhibited SET (see Figure 2).

The equivalent resistance and capacitance can be extracted using the DBTJ model of equivalent circuitry and the least-squares fitting of the *I*–*V* measurements following prior reports.[6,10,22,32] The capacitance, $C = C_1 + C_2$, of the NPs can be calculated from the width of the CB (ΔV) using $\Delta V = e/C$.[7,33] For the P20 NP shown in Figure 2, ΔV = 1.06 V and C =

0.15 aF. The resistances of the two junctions extracted from the fitting (Figure 2) are summarized in Table 1. The asymmetric shape of the current at negative versus positive biases suggests the existence of a nonzero value of fractional charge (Q_0) of 0.05 e on the NP.[3,6] Assuming that the SET is from one Au single-crystal particle, we could estimate the particle size from the measured capacitance, $C = 0.15$ aF $= 2\pi d\varepsilon_0\varepsilon$, where ε of the alkanethiol SAM is 2.7.[34] The size of the P20 NP, d_{P20}, therefore equals 1.0 nm. The particle standing alone should exhibit SET characteristics. This exercise indicates that the SET observed is due to a subdomain of 1.0 nm, despite the overall particle dimension of 20 nm. To the best of our knowledge, these measurements provide the first unambiguous proof that the small domains within the polycrystalline Au NPs are sufficiently isolated from the rest of the particle, thus leading to SET behavior. In other words, the SET is independent of the overall polycrystalline NP size.

Corroborative evidence of the presence of subparticulate domains can be found from high-resolution TEM (HRTEM) imaging, as shown in Figure 3A. The TEM contrast of the P20 NP contains multiple crystalline grains, some marked by yellow dash frames. Further support of polycrystalline grains arises from spectroscopic investigations, including laser scanning confocal microscopy (LSCM) imaging and spectroscopy and X-ray photoelectron spectroscopy (XPS). Under excitation of 514 nm, the spectrum of the P20 NPs is shown in Figure 3B, revealing an emission peak from 630–670 nm. On the basis of the correlation between the number of atoms in an Au quantum dot and the emission energy, the emission range of 630–670 nm can be ascribed to Au nanocrystals consisting of 13–23 atoms,[35] which corresponds to nanocrystals of 0.75 to 0.91 nm assuming spherical geometry. Our prior XPS study of P20 NPs reported an additional Au $4f_{7/2}$ peak at 85.1 eV in comparison with C20 NPs, which also points to the existence of 1 nm grains.[27,28]

This Letter reports the first observation of SET from tens of nanometer sized metallic NPs at room temperature, which breaks the conventional size limit of 10 nm for a metallic NP to show SET at room temperature. This was done by using engineered polycrystalline Au NPs. The SET observed derives from the ultrasmall single crystalline grain(s) within the polycrystal, which is (are) sufficiently isolated from the nearest neighbor grains. In other words, the nanocomposite materials may be engineered to preserve the overall integrity of the particle yet maintain the individual grains' properties. Work is in progress to vary the engineering parameters and investigate the individual and overall properties of the nanocomposites.

EXPERIMENTAL METHODS

Materials

Glycine (≥99%), $KAuCl_4$ (98%), $Na_2B_4O_7$ (≥99.5%), NaOH (≥98%), 1-decanethiol (C10S) (99%), 1-octanethiol (C8S) (≥98.5%), 1,8-octanedithiol (C8S2) (≥97%), 4,4′-bis(mercaptomethyl)biphenyl (BMMBP) (97%), 2-aminoethanethiol (AET) (98%), methanol (99.8%), toluene (99.8%), and hexane (95%) were purchased from Sigma-Aldrich (St. Louis, MO). Au slugs (99.999%) were purchased from Alfa Aesar (Ward Hill, MA). Ethanol (99.99%) was purchased from Gold Shield Chemical (Hayward, CA). Water (≥18.2 MΩ) was generated from a Milli-Q system (Q-GARD 2, Millipore, Billerica, MA) and used

for dilution and washing. Nitrogen gas (99.999%) was purchased from Praxair (Danbury, CT). Tungsten wire (99.95%) was purchased from California Fine Wire (Grover Beach, CA). All chemicals and materials were used without further purification.

Three Types of Au NPs

Polycrystalline NPs (P20 NPs) were synthesized using the solid-state glycine matrices method we previously reported.[28] In brief, 250 mg of glycine and 13 mg of $KAuCl_4$ were codissolved in 1.5 mL of water. Subsequently, the solution was nitrogen blown dry and the mixture was reduced at 453 K. The reaction was stopped when the color became dark reddish and the product was dissolved in 1 mL of water. The solution was centrifuged at 2000 *g* for 2 min then 4000 *g* for 2 min to remove the large aggregates. The supernatant was collected and further centrifuged at 7000 *g* for 3 min. Finally, the pellet was collected and redissolved in 10 mM $Na_2B_4O_7$ buffer.

Ultrasmall (core size <2 nm) single-crystal Au NPs (S1.5 NPs) were synthesized following previously published procedures.[29,36] In brief, Au NPs were synthesized by the Brust reaction,[36] followed by size fractionation and thermal annealing to ensure a narrow distribution of the desired particle size. This step yielded single-crystal NPs with a core size of 1.5 nm coated by C8S in toluene. Subsequently, the initial surfactant coatings were replaced by C8S2 through an exchange reaction upon adding hexane-dissolved C8S2.[29] Excess C8S2 ligands were removed by repeated extraction with methanol after the exchange reaction. The final product was dispersed in hexane for further use. NPs produced in this method exhibit little to no carbon residue, as the characteristic Raman peak (1600 cm^{-1}) of carbon residues was never observed from SERS spectrum of glycine-coated polycrystalline gold nanoparticles.[28]

Conventional NPs (20 nm in core, C20 NPs), coated with citrate and dispersed in H_2O, were purchased from ASEMBLON (Redmond, WA). Their size was measured via TEM to allow comparison with our P20 NP systems.

Characterization of the Core Size and Crystallinity of Au NPs via HRTEM Imaging

TEM images were obtained using a JEOL 2100 transmission electron microscope (Pleasanton, CA) with a 200 kV accelerating voltage and a point resolution of 0.23 nm. For TEM sample preparation, a solution of 1 nM Au NPs was drop cast onto a carbon-coated copper grid purchased from TED PELLA (Redding, CA) and allowed to dry.

The TEM imaging revealed the core size and narrow distribution of the P20 NPs, C20 NPs, and S1.5 NPs to be 20.0 ± 0.9, 20.2 ± 1.5, and 1.5 ± 0.4 nm, respectively. The analysis of TEM fringes revealed that (1) S1.5 NPs are single crystalline, (2) P20 NPs are polycrystalline containing grains with sizes of down to 1 nm, and (3) C20 NPs contain grains with size ≥8 nm.[27]

Immobilization of NPs on Surfaces for AFM and STM Imaging

Au(111) thin films were prepared and served as supports and electrodes for NPs. These films were produced in a high vacuum evaporator (model DV502-A, Denton Vacuum,

Moorestown, NJ) following previously reported procedures.[26,37] Freshly cleaved mica was preheated to 350 °C. At background pressure of 10^{-7} Torr, an Au slug was heated into vapor phase, which deposited onto the mica(0001) surfaces. Evaporations were stopped when the thickness reached 200 nm and were followed by annealing at 350 °C for 20 min. Immediately before soaking in a designated thiol solution, the Au films were treated with H_2 flaming to decontaminate and enlarge Au(111) terraces.

AET SAMs were prepared by immersion of freshly hydrogen flamed Au electrodes in AET solution (1 mM in ethanol) for 24 h, followed by ethanol and hexane rinses, and dried in nitrogen. BMMBP SAMs were prepared following the same protocol. Immersion of the BMMBP SAM in a S1.5 NP solution (0.5 mg/mL) for 5 min allowed ~40% coverage of Au NPs on the surfaces. S1.5 NPs were immobilized on the electrode through chemisorption between the Au cores of the NPs and the terminal thiol groups from the BMMBP SAM.[3,38]

P20 NPs and C20 NPs were immobilized following similar protocols as S1.5, using AET SAMS, and a soaking time of 3 h. The stability of surface supported C20 NPs was due to the electrostatic attraction of the citrate coating with the amine termini of the AET SAM.[38] Similar immobilization occurred between the glycine coating of P20 NPs and the amine termini of SAMs. Finally, the samples were immersed in C10S ethanol solution (0.1 mM) for 10 min just prior to STM investigation in UHV to passivate defects within the SAMs.

Characterization of the Overall Particle Size via AFM Imaging

AFM images were acquired using an MFP-3D AFM (Asylum Research, Santa Barbara, CA). Imaging was performed under tapping mode with silicon cantilevers (AC-240, Olympus, spring constant 1 N/m), and the damping was set to 80%. Images were acquired at a scanning speed of 1.25 μm/s and a pixel size of 256 × 256 and analyzed using Asylum MFP-3D software developed on the Igor Pro 6.34 platform. The overall sizes of P20, C20, and S1.5 NPs, measured from their height in topographic images, were 20.9 ± 0.9, 21.1 ± 1.0, and 2.3 ± 0.1 nm, respectively, which are consistent with the Au particle cores' diameters 20.0 ± 0.9, 20.2 ± 1.5, and 1.5 ± 0.4 nm, respectively.

STM Imaging and I–V Measurements

The STM operates under UHV (STM100, RHK Technology, Troy, MI) with a base pressure of 5×10^{-10} Torr. The STM tips were made from a 0.01 in. tungsten wire, cut and sharpened by electrochemical etching in a 3 M NaOH solution.[25] Prior to *I–V* measurements, STM images of surface bound NPs were imaged under voltage of 0.5 to 1.0 V, where the typical tunneling current range was 5–40 pA. From STM topographs, we selected the particles that were characteristic of the systems and relatively isolated from the high coverage regions. The sizes of the selected NPs were measured from the height in the STM topographs. Because STM height is convoluted with the local density of state,[39] we calibrated the STM height by acquiring STM images of identical samples that had AFM images taken of them. The size distributions of the three Au NPs systems selected for this investigation were very narrow: For example, in the case of P20 NPs, there was 4.5% dispersion of Au core size based on TEM imaging and 4.3% dispersion of overall size based on AFM measurements. With this narrow distribution, our calibration is accurate up to 1 nm. Upon selection of a NP,

the tip was parked over the center of the particle, and *I*–*Z* measurements were taken, typically at 1.0 V and 30 pA, from which the contact point and tip-particle separation were determined.[6] The tip was then parked at the designed separation, and *I*–*V* measurements were acquired at a rate of 20 V/s. The numerical fitting of the *I*–*V* spectrum using the DBTJ model was performed using SETNETS freeware.[39,40]

Confocal Spectroscopy

Emission spectra of P20 NPs were acquired by LSCM (Olympus Fluoview 1000, Olympus America, Central Valley, PA) using a Plan Apo N (60×, NA = 1.42) oil-immersion bright-field objective with a working distance of 0.15 mm. P20 NPs were drop cast onto a glass slide, followed by drying in air before being studied by LSCM. For the emission spectra acquired, NPs were illuminated via 514 nm excitation at 8.9 mW.

ACKNOWLEDGMENTS

We gratefully acknowledge helpful discussions with Professor Li Tan at University of Nebraska, Lincoln. This work is supported by the Gordon and Betty Moore Foundation, National Science Foundation (DMR–1104260), National Institutes of Health (1R21 ES025350-01A1 and 1R21EB011762), and W. M. Keck Foundation.

REFERENCES

(1). Kano S, Tada T, Majima Y. Nanoparticle Characterization Based on STM and STS. Chem. Soc. Rev. 2015; 44:970–987. [PubMed: 25306971]

(2). Feldheim DL, Keating CD. Self-assembly of Single Electron Transistors and Related Devices. Chem. Soc. Rev. 1998; 27:1–12.

(3). Andres RP, Bein T, Dorogi M, Feng S, Henderson JI, Kubiak CP, Mahoney W, Osifchin RG, Reifenberger R. Coulomb Staircase at Room Temperature in a Self-Assembled Molecular Nanostructure. Science. 1996; 272:1323–1325. [PubMed: 8662464]

(4). Braun E, Eichen Y, Sivan U, Ben-Yoseph G. DNA-Templated Assembly and Electrode Attachment of a Conducting Silver Wire. Nature. 1998; 391:775–778. [PubMed: 9486645]

(5). Chen S, Ingram RS, Hostetler MJ, Pietron JJ, Murray RW, Schaaff TG, Khoury JT, Alvarez MM, Whetten RL. Gold Nanoelectrodes of Varied Size: Transition to Molecule-Like Charging. Science. 1998; 280:2098–2101. [PubMed: 9641911]

(6). Yang G, Tan L, Yang Y, Chen S, Liu G-Y. Single Electron Tunneling and Manipulation of Nanoparticles on Surfaces at Room Temperature. Surf. Sci. 2005; 589:129–138.

(7). Brousseau LC, Zhao Q, Shultz DA, Feldheim DL. pH-Gated Single-Electron Tunneling in Chemically Modified Gold Nanoclusters. J. Am. Chem. Soc. 1998; 120:7645–7646.

(8). Chung S-W, Ginger DS, Morales MW, Zhang Z, Chandrasekhar V, Ratner MA, Mirkin CA. Top-Down Meets Bottom-Up: Dip-Pen Nanolithography and DNA-Directed Assembly of Nanoscale Electrical Circuits. Small. 2005; 1:64–69. [PubMed: 17193349]

(9). Nijhuis CA, Oncel N, Huskens J, Zandvliet HJW, Ravoo BJ, Poelsema B, Reinhoudt DN. Room-Temperature Single-Electron Tunneling in Dendrimer-Stabilized Gold Nanoparticles Anchored at a Molecular Printboard. Small. 2006; 2:1422–1426. [PubMed: 17192998]

(10). Wang B, Wang H, Li H, Zeng C, Hou JG, Xiao X. Tunable Single-Electron Tunneling Behavior of Ligand-Stabilized Gold Particles on Self-Assembled Monolayers. Phys. Rev. B: Condens. Matter Mater. Phys. 2000; 63:035403.

(11). Dubois JGA, Gerritsen JW, Shafranjuk SE, Boon EJG, Schmid G, van Kempen H. Coulomb Staircases and Quantum Size Effects in Tunnelling Spectroscopy on Ligand-Stabilized Metal Clusters. Europhys. Lett. 1996; 33:279.

(12). Bigioni TP, Harrell LE, Cullen WG, Guthrie DK, Whetten RL, First PN. Imaging and Tunneling Spectroscopy of Gold Nanocrystals and Nanocrystal Arrays. Eur. Phys. J. D. 1999; 6:355–364.

(13). Harrell LE, Bigioni TP, Cullen WG, Whetten RL, First PN. Scanning Tunneling Microscopy of Passivated Au Nanocrystals Immobilized on Au(111) Surfaces. J. Vac. Sci. Technol., B: Microelectron. Process. Phenom. 1999; 17:2411–2416.

(14). Jiang P, Liu ZF, Cai SM. In Situ CdS Nanocluster Formation on Scanning Tunneling Microscopy Tips for Reliable Single-Electron Tunneling at Room Temperature. Appl. Phys. Lett. 1999; 75:3023–3025.

(15). Graf H, Vancea J, Hoffmann H. Single-Electron Tunneling at Room Temperature in Cobalt Nanoparticles. Appl. Phys. Lett. 2002; 80:1264–1266.

(16). Simon U. Charge Transport in Nanoparticle Arrangements. Adv. Mater. 1998; 10:1487–1492.

(17). Ray V, Subramanian R, Bhadrachalam P, Ma L-C, Kim C-U, Koh SJ. CMOS-Compatible Fabrication of Room-Temperature Single-Electron Devices. Nat. Nanotechnol. 2008; 3:603–608. [PubMed: 18838999]

(18). Jiang P, Liu Z-F, Cai S-M. Single-Electron Tunneling in a Single PbS Nanocrystal Nucleated on 11-Mercaptoundecanoic Acid Self-Assembled Monolayer at Room Temperature. J. Appl. Phys. 2001; 90:2039–2041.

(19). Yun M, Ramalingam B, Gangopadhyay S. Room Temperature Observation of Size Dependent Single Electron Tunneling in a Sub-2 nm Size Tunable Pt Nanoparticle Embedded Metal–Oxide–Semiconductor Structure. Nanotechnology. 2011; 22:465201. [PubMed: 22024690]

(20). Schmid G, Liu Y-P, Schumann M, Raschke T, Radehaus C. Quasi One-Dimensional Arrangements of $Au_{55}(PPh_3)_{12}Cl_6$ Clusters and Their Electrical Properties at Room Temperature. Nano Lett. 2001; 1:405–407.

(21). Feldheim DL, Grabar KC, Natan MJ, Mallouk TE. Electron Transfer in Self-Assembled Inorganic Polyelectrolyte/Metal Nanoparticle Heterostructures. J. Am. Chem. Soc. 1996; 118:7640–7641.

(22). Chaki NK, Singh P, Dharmadhikari CV, Vijayamohanan KP. Single-Electron Charging Features of Larger, Dodecanethiol-Protected Gold Nanoclusters: Electrochemical and Scanning Tunneling Microscopy Studies. Langmuir. 2004; 20:10208–10217. [PubMed: 15518515]

(23). Doty RC, Yu H, Shih CK, Korgel BA. Temperature-Dependent Electron Transport through Silver Nanocrystal Superlattices. J. Phys. Chem. B. 2001; 105:8291–8296.

(24). Liu G-Y, Xu S, Qian Y. Nanofabrication of Self-Assembled Monolayers Using Scanning Probe Lithography. Acc. Chem. Res. 2000; 33:457–466. [PubMed: 10913234]

(25). Riposan A, Liu G.-y. Significance of Local Density of States in the Scanning Tunneling Microscopy Imaging of Alkanethiol Self-Assembled Monolayers. J. Phys. Chem. B. 2006; 110:23926–23937. [PubMed: 17125360]

(26). Yang G, Liu G.-y. New Insights for Self-Assembled Monolayers of Organothiols on Au(111) Revealed by Scanning Tunneling Microscopy. J. Phys. Chem. B. 2003; 107:8746–8759.

(27). Zheng J, Zhou C, Yu M, Liu J. Different Sized Luminescent Gold Nanoparticles. Nanoscale. 2012; 4:4073–4083. [PubMed: 22706895]

(28). Zhou C, Yu J, Qin Y, Zheng J. Grain Size Effects in Polycrystalline Gold Nanoparticles. Nanoscale. 2012; 4:4228–4233. [PubMed: 22456680]

(29). Chen S. Self-Assembling of Monolayer-Protected Gold Nanoparticles. J. Phys. Chem. B. 2000; 104:663–667.

(30). Kleibert A, Rosellen W, Getzlaff M, Bansmann J. Structure, Morphology, and Magnetic Properties of Fe Nanoparticles Deposited onto Single-Crystalline Surfaces. Beilstein J. Nanotechnol. 2011; 2:47–56. [PubMed: 21977415]

(31). Barbet J, Garvin A, Thimonier J, Chauvin J-P, Rocca-Serra J. Scanning Tunneling Microscopy of Colloidal Gold Beads. Ultramicroscopy. 1993; 50:355–363.

(32). Fleming CJ, Liu YX, Deng Z, Liu G.-y. Deformation and Hyperfine Structures of Dendrimers Investigated by Scanning Tunneling Microscopy. J. Phys. Chem. A. 2009; 113:4168–4174. [PubMed: 19278254]

(33). Berven CA, Clarke L, Mooster JL, Wybourne MN, Hutchison JE. Defect-Tolerant Single-Electron Charging at Room Temperature in Metal Nanoparticle Decorated Biopolymers. Adv. Mater. 2001; 13:109–113.

(34). Rampi MA, Schueller OJA, Whitesides GM. Alkanethiol Self-Assembled Monolayers as the Dielectric of Capacitors with Nanoscale Thickness. Appl. Phys. Lett. 1998; 72:1781–1783.

(35). Zheng J, Zhang C, Dickson RM. Highly Fluorescent, Water-Soluble, Size-Tunable Gold Quantum Dots. Phys. Rev. Lett. 2004; 93:077402. [PubMed: 15324277]

(36). Brust M, Walker M, Bethell D, Schiffrin DJ, Whyman R. Synthesis of Thiol-Derivatised Gold Nanoparticles in a Two-Phase Liquid-Liquid System. J. Chem. Soc., Chem. Commun. 1994; 801:802.

(37). Qian Y, Yang G, Yu J, Jung TA, Liu G.-y. Structures of Annealed Decanethiol Self-Assembled Monolayers on Au(111): an Ultrahigh Vacuum Scanning Tunneling Microscopy Study. Langmuir. 2003; 19:6056–6065.

(38). Zhao J, Terfort A, Zharnikov M. Gold Nanoparticle Patterning on Monomolecular Chemical Templates Fabricated by Irradiation-Promoted Exchange Reaction. J. Phys. Chem. C. 2011; 115:14058–14066.

(39). Hansma PK, Tersoff J. Scanning Tunneling Microscopy. J. Appl. Phys. 1987; 61:R1–R24.

(40). Hadley, P. [accessed November 2015] http://lamp.tu-graz.ac.at/~hadley/set/asymIV/SETIV.html

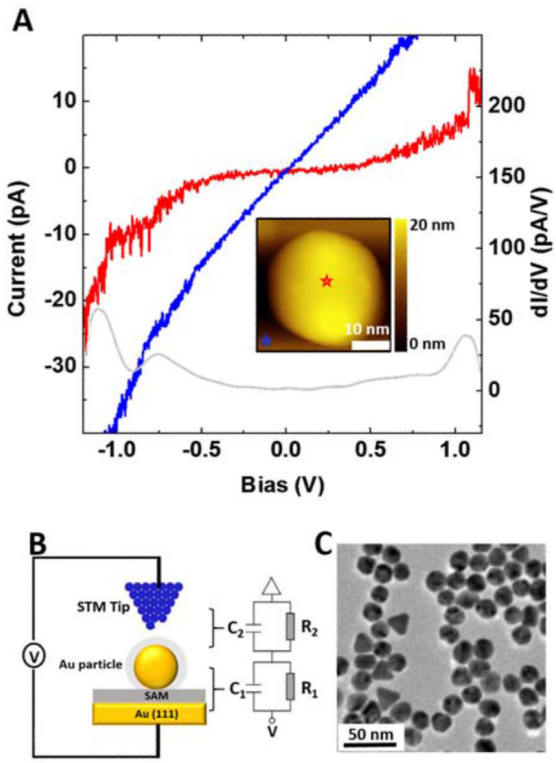

Figure 1.

(A) *I–V* measurement of a P20 NP (see inset for its image) at tip-NP separation of 0.03 nm (red curve). An *I–V* measurement of the surrounding SAM is displayed in the same plot for comparison (tip-SAM separation 0.08 nm, blue curve). Red and blue stars indicate the locations above which the *I–V* curves were acquired for the NP and SAM, respectively. (B) Schematic illustration (left) of the SET measurements using STM imaging and spectroscopy, displayed with the corresponding equivalent circuit and the double-barrier tunneling junction (DBTJ) model (right). (C) TEM image of P20 NPs, representing the characteristic distribution of the particle size.

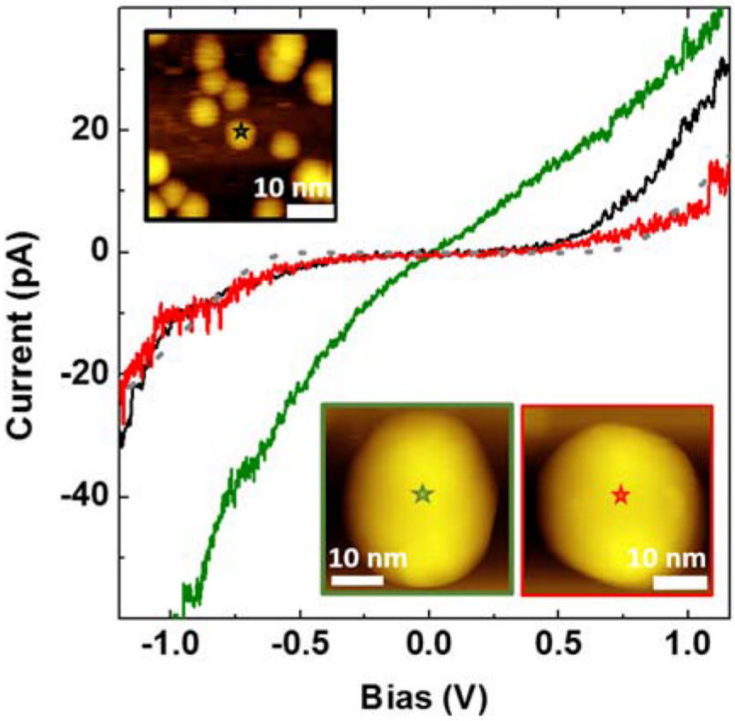

Figure 2.

STS *I–V* characteristics of a single P20 NP (red), C20 NP (green), and S1.5 NP (black) obtained at tip-NP separations of 0.03, 0.03, and 0.12 nm, respectively. Insets are STM images of the NPs, where the red, green, and black stars indicate the locations above which the *I–V* curves were acquired for P20, C20, and S1.5 NPs, respectively. The lateral dimension in the STM images appears larger than 20 nm due to tip convolution effects.[30,31] Fitting (gray dashed line) of the *I–V* curve of the P20 NP based on the DBTJ model is shown in the same plot.

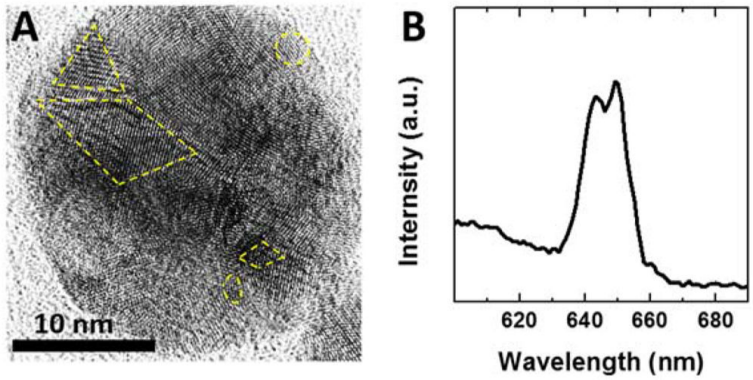

Figure 3.

HRTEM images of a single P20 NP (A). Emission spectra of P20 NPs obtained by LSCM at excitation of 514 nm (B).

Table 1

Capacitance, Resistance, and Apparent Particle Size Based on *I–V* Measurements and Least-Square Fitting Using DBTJ Circuit for the P20 NP Shown in Figure 2

***I–V* curve observation**		**SET numerical fitting**		**apparent NP size**
CB width 1.06 V	R_1 = 1 GΩ	R_2 = 16 GΩ	Q_0 = 0.05 e	d = 1.0 nm
$C = C_1 + C_2$ = 0.15 aF	C_1 = 0.11 aF	C_2 = 0.04 aF		